Hindawi
Advances in Multimedia
Volume 2023, Article ID 9764043, 1 page
https://doi.org/10.1155/2023/9764043

Retraction

Retracted: Application Effect Analysis of the Mie Scattering Theory Based on Big Data Analysis Technology in the Optical Scattering Direction

Advances in Multimedia

Received 15 August 2023; Accepted 15 August 2023; Published 16 August 2023

This article has been retracted by Hindawi following an investigation undertaken by the publisher [1]. This investigation has uncovered evidence of one or more of the following indicators of systematic manipulation of the publication process:

(1) Discrepancies in scope
(2) Discrepancies in the description of the research reported
(3) Discrepancies between the availability of data and the research described
(4) Inappropriate citations
(5) Incoherent, meaningless and/or irrelevant content included in the article
(6) Peer-review manipulation

The presence of these indicators undermines our confidence in the integrity of the article's content and we cannot, therefore, vouch for its reliability. Please note that this notice is intended solely to alert readers that the content of this article is unreliable. We have not investigated whether authors were aware of or involved in the systematic manipulation of the publication process.

Wiley and Hindawi regrets that the usual quality checks did not identify these issues before publication and have since put additional measures in place to safeguard research integrity.

We wish to credit our own Research Integrity and Research Publishing teams and anonymous and named external researchers and research integrity experts for contributing to this investigation.

The corresponding author, as the representative of all authors, has been given the opportunity to register their agreement or disagreement to this retraction. We have kept a record of any response received.

References

[1] S. Chen, "Application Effect Analysis of the Mie Scattering Theory Based on Big Data Analysis Technology in the Optical Scattering Direction," *Advances in Multimedia*, vol. 2022, Article ID 6158067, 10 pages, 2022.

Hindawi
Advances in Multimedia
Volume 2022, Article ID 6158067, 10 pages
https://doi.org/10.1155/2022/6158067

Research Article

Application Effect Analysis of the Mie Scattering Theory Based on Big Data Analysis Technology in the Optical Scattering Direction

Suting Chen

Shanghai Jian Qiao University, College of Education, Shanghai 201306, China

Correspondence should be addressed to Suting Chen; chenst@gench.edu.cn

Received 25 July 2022; Revised 29 August 2022; Accepted 6 September 2022; Published 20 September 2022

Academic Editor: Tao Zhou

In order to study the characteristics of wake, an application method of the Mie scattering theory based on big data analysis technology in the optical scattering direction is proposed in this paper. Firstly, based on the scattering theory, the optical scattering model of a single bubble is simulated on the computer. It is concluded that the light scattering properties of a single bubble are closely related to the bubble diameter and relative refractive index. Based on the single bubble scattering model, the properties of bubble group scattering are further discussed. Under the condition of irrelevant scattering, the scattering of the bubble group satisfies the linear superposition of single bubble scattering. Under the assumed mathematical model of bubble group scattering, the scattered light intensity of wake can be measured experimentally, and then, the velocity, diameter, and density distribution of the bubble group can be calculated by using the mathematical inversion algorithm. The experimental results show that the diameter of the main bubbles in the bubble group is about 240, accounting for about 50% of the whole bubble group in number, the bubbles with a diameter of about 140 account for 24% of the whole bubble group, and the bubbles with a diameter of about 350 account for 24% of the whole bubble group. *Conclusion*. It is feasible to detect the wake by the backscattered light of the wake.

1. Introduction

The motion of a ship in the ocean will disturb the sea water and form a wake behind the ship. Due to the rotating cavitation of the propeller, the breaking of sea waves, and the involvement of a large amount of air in the waterline, a bubble curtain belt containing a large number of bubbles is formed in the seawater at the tail of the ship, which is commonly referred to as bubble wake [1]. From the perspective of physics, wake has acoustic, thermal, optical, magnetic, and electrical characteristics. The number of bubbles in the wake is huge and their diameters are different. Among them, large bubbles will rise quickly, break, and disappear, while small bubbles can survive in seawater for more than ten minutes or even dozens of minutes [2]. Due to the obvious difference of bubble density, compressibility, and other parameters from seawater and the influence of turbulence in the wake, the bubble distribution in the wake is uneven, which leads to the obvious difference between the transmission characteristics of sound wave and light wave in the wake and that in seawater. Therefore, as long as these characteristics can be mastered, they can be used as the basis for detecting the wake acoustic characteristics. It mainly studies the absorption and scattering characteristics of sound through the wake, including bubbles. Although this theory is not widely accepted, it is widely used because there is no more perfect theory. The thermal characteristics of wake are based on its influence on the temperature distribution of seawater. At present, thermocouples are often used to measure. However, the research on the optical characteristics of wake is still in its infancy in China because of military secrets, which have not been reported abroad for practicality [3]. This research can further grasp the wake structure and physical properties in theory and promote the development of military detection in practice. It can also be applied to water quality detection and other fields. Therefore, the research on the optical characteristics of wake has important theoretical and practical significance.

2. Literature Review

Xiao et al. found that the scattering of bubbles in water conforms to the Mie scattering theory according to Mie scattering research. The Mie scattering theory has become the main method to study the light scattering properties of bubbles in water. At this time, Marston applied the Mie scattering theory to study the distribution and detection of the single bubble size [4]. Yan et al. used the scattering theory to study the backscattering of the ocean and the number and size distribution of submicron particles [5]. Li et al. began to use the scattering theory to study the optical characteristics of bubble groups in the ocean. Through their research, they came to the conclusion that the contribution of bubbles to the scattering and backscattering of light in seawater can reach approximately 10% and obtained the distribution of the bubble size by using the holographic technology [6]. McGrory et al. estimated the optical properties of clean bubbles and bubbles covered with thin layers of organic matter with the Mie scattering theory. The results showed that in the visible light range, the light scattering properties of bubbles covered with thin layers of organic matter and pure bubbles were similar, but its backscattering coefficient was much larger than that of pure bubbles [7]. Li et al. theoretically studied and analyzed the bubble water with uneven size by establishing the acoustic physical model of bubble water, quoting Rayleigh-Plesset equation, analyzed the attenuation coefficient and nonlinear equivalent parameters of sound waves in bubble water, and concluded that the second harmonic in bubble water is close to zero, but this conclusion needs to be further verified [8]. Bhullar et al. used the marine experiment site to measure the influence of the wake bubble group of the ship on the optical characteristics of the sea water (such as remote sensing reflectance and normalized water leaving radiance), providing a theoretical basis for obtaining the wake information of the ship through remote sensing of spaceborne optical sensors [9]. It is proved that in the visible and near-infrared bands, the ship's bubble containing wake changes the remote sensing reflectivity of the seawater not only in the amplitude but also in the spectral shape. As a result, the wake bubble makes the sea water greener. At the same time, as the position of the observation point in the wake is close to the target ship, the bubble density continues to increase, and the reflectivity also increases. Through experiments, the practical significance of using the optical characteristics of wake bubbles to track ships is directly proved, and the significance of the study of wake bubbles is also proved from the side. Based on the study of the light scattering properties of a single bubble, the scattering theory is applied to the light scattering of bubbles. Firstly, based on the scattering theory, the optical scattering model of a single bubble is simulated on the computer. It is concluded that the light scattering properties of a single bubble are closely related to the bubble diameter and relative refractive index. Based on the single bubble scattering model, the properties of bubble group scattering are further discussed. Under the condition of irrelevant scattering, the scattering of the bubble group satisfies the linear superposition of single bubble scattering. Under the assumed mathematical model of the bubble group scattering, the scattered light intensity of wake can be measured experimentally, and then, the velocity, diameter, and density distribution of the bubble group can be calculated by using the mathematical inversion algorithm.

3. Research Methods

3.1. Mie Scattering. Light scattering refers to the light phenomenon that light deviates from its original propagation direction and spreads to all directions through an uneven medium, as shown in Figure 1. When light propagates in a uniform medium, the light propagates along the original direction of incident light without scattering. However, when light passes through an uneven medium, these uneven particles in the medium will cause scattering effects. The intensity distribution of this kind of scattered light is related to the size, refractive index, and incident wavelength of scattering particles. The micron scale bubble scattering problem is very suitable to be explained by the Mie scattering theory. The Mie scattering theory is a strict mathematical solution of Maxwell's equation for homogeneous particles in uniform media under the irradiation of plane monochromatic waves [10].

According to the Mie scattering, the scattered light intensity of point a at the distance from the scatterer is as follows:

$$I_{\text{sca}} = I_0 \frac{\lambda^2}{8\pi^2 r^2} I(\theta, \phi), \tag{1}$$

$$I(\theta, \phi) = |S_1(\theta)|^2 \sin^2\phi + |S_2(\theta)|^2 \cos^2\phi. \tag{2}$$

In formula (1), $I(\theta, \phi)$ represents the scattered light intensity, I_0 represents the incident light intensity, λ represents the incident light wavelength, θ represents the scattering angle, and ϕ represents the polarization angle of polarized light. In formula (2), $S_1(\theta)$ and $S_2(\theta)$ are amplitude functions, and their specific expressions are as follows:

$$S_1(\theta) = \sum_{n=1}^{\infty} \frac{2n+1}{n(n+1)} [\mathrm{a}_n \pi_n + \mathrm{b}_n \tau_n], \tag{3}$$

$$S_2(\theta) = \sum_{n=1}^{\infty} \frac{2n+1}{n(\mathrm{n}+1)} [\mathrm{a}_n \tau_n + \mathrm{b}_n \pi_n]. \tag{4}$$

In (3) and (4), a_n and b_n are functions related to the Bessel function and Hankel function, respectively, and π_n and τ_n are functions related to associated Legendre function only related to scattering angle θ, as shown in the following formula:

$$a_n = \frac{\varphi_n(\alpha)\varphi_n'(m\alpha) - m\varphi_n'(\alpha)\varphi_n(m\alpha)}{\varepsilon_n(\alpha)\varphi_n'(m\alpha) - m\varepsilon_{nn}'(\alpha)\varphi_n(m\alpha)}, \tag{5}$$

$$b_n = \frac{m\varphi_n(\alpha)\varphi_n'(m\alpha) - \varphi_n'(\alpha)\varphi_n(m\alpha)}{m\varepsilon_n(\alpha)\varphi_n'(m\alpha) - \varepsilon_n'(\alpha)\varphi_n(m\alpha)}. \tag{6}$$

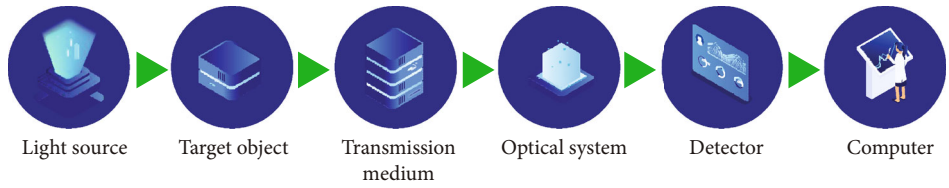

Figure 1: Light scattering.

In formulas (5) and (6), $\varphi_n(\alpha)$ and $\varepsilon_n(\alpha)$ are the Bessel functions and Hankel functions of the first kind, respectively, where a is the dimensionless diameter and $\alpha = \pi D/\lambda$, D is the actual diameter of the particle, λ is the wavelength of the incident light in vacuum, and m is the refractive index of the particle relative to the surrounding medium.

From the above formula, it can be analyzed that the key to the calculation of light intensity distribution of the Mie scattering formula is the calculation of a_n and b_n, which is an infinite approaching process. Studying the calculation algorithm of Mie scattering, these two scattering coefficients are one of the important research directions of the Mie scattering theory [11].

The scattering coefficient of Mie scattering satisfies the following recursive formula:

$$\begin{aligned}
\varphi_n(\alpha) &= \frac{2n-1}{\alpha}\varphi_{n-1}(\alpha) - \varphi_{n-2}(\alpha),\\
\varphi_n'(\alpha) &= -\frac{n}{\alpha}\varphi_{n-1}(\alpha) - \varphi_{n-2}(\alpha),\\
\varepsilon_n(\alpha) &= \frac{2n-1}{\alpha}\varepsilon_{n-1}(\alpha) - \varepsilon_{n-2}(\alpha),\\
\varepsilon_n'(\alpha) &= -\frac{n}{\alpha}\varepsilon_n(\alpha) + \varepsilon_{n-1}(\alpha).
\end{aligned} \tag{7}$$

Its initial value is as follows:

$$\begin{aligned}
\varphi_{-1}(\alpha) &= \cos\alpha,\\
\varphi_0(\alpha) &= \sin\alpha,\\
\tau_n &= \pi_n\cos\theta - \pi_n'\sin^2\theta,\\
\varepsilon_{-1}(\alpha) &= \cos\alpha - i\sin\alpha,\\
\varepsilon_0(\alpha) &= \sin\alpha + i\cos\alpha,\\
\pi_0 &= 0,\\
\pi_1 &= 1,\\
\pi_n &= \frac{2n-1}{n-1}\pi_{n-1}\cos\theta - \frac{n}{n-1}\pi_{n-2},\\
\pi_n' &= (2n-1)\pi_{n-1} + \pi_{n-2}',\\
\pi_0' &= \pi_1' = 0.
\end{aligned} \tag{8}$$

From the above recurrence relationship and output value, the distribution coefficient of Mie scattering light intensity can be calculated by a computer, and then, the Mie scattering light intensity distribution can be obtained.

The classical Mie scattering formula is the scattering light intensity analysis of particles in homogeneous medium under plane light irradiation. The Mie scattering formula under Gaussian beam TE_{00} mode irradiation in absorbing medium should be further improved and optimized, as shown in

$$\begin{aligned}
S_1(\theta) &= \sum_{n=1}^{\infty}\frac{2n+1}{n(n+1)}\left[a_n^m\pi_n + b_n^m\tau_n\right],\\
S_2(\theta) &= \sum_{n=1}^{\infty}\frac{2n+1}{n(\mathrm{n}+1)}\left[\mathrm{a}_n^m\tau_n + \mathrm{b}_n^m\pi_n\right],
\end{aligned} \tag{9}$$

where $a_n^m = a_n g_{n,TE}^m$, $b_n^m = b_n g_{n,TM}^m$, $g_{n,TE}^m$, and $g_{n,TM}^m$ are the beam diffusion coefficients of Gaussian beams in the spherical coordinate system. The other expressions remain unchanged, but the meaning of parameters in the smart media changes. The specific expression is as follows:

$$\begin{aligned}
a_n &= \frac{\varphi_n(\alpha)\varphi_n'(m\alpha) - m\varphi_n'(\alpha)\varphi_n(m\alpha)}{\varepsilon_n(\alpha)\varphi_n'(m\alpha) - m\varepsilon_n'(\alpha)\varphi_n(m\alpha)},\\
b_n &= \frac{m\varphi_n(\alpha)\varphi_n'(m\alpha) - \varphi_n'(\alpha)\varphi_n(m\alpha)}{m\varepsilon_n(\alpha)\varphi_n'(m\alpha) - \varepsilon_n'(\alpha)\varphi_n(m\alpha)}.
\end{aligned} \tag{10}$$

In formula (10), $\alpha = 2\pi D m_{\mathrm{med}}/\lambda$, where D is the actual diameter of the particle, λ is the incident wavelength, and m_{med} is the refractive index of the surrounding medium.

As shown in Figure 2, curves A, B, and C correspond to the Mie extinction coefficient under different refractive indexes of the medium. The absorption coefficient of the medium will affect the extinction coefficient of Mie scattering and the final light intensity distribution. However, in general, the extreme value and distribution law of light intensity distribution have not been affected. In the inversion calculation, the relative value of the optimization algorithm can be used to solve the influence of different coincidence coefficients of the medium [12].

Figure 3 is the program flow chart.

3.2. Simulation of Backscattered Light Signal of Underwater Bubble. When the size of particles is much larger than the size of photons, the Mie scattering theory can be used to establish a model. Bubbles are small-radius particles, but their size is much larger than that of photons, so the process of photons emitted onto bubbles and scattered can apply the Mie scattering theory. According to the meter scattering formula, the distributed scattering intensity under a different bubble radius can be calculated when the light wavelength

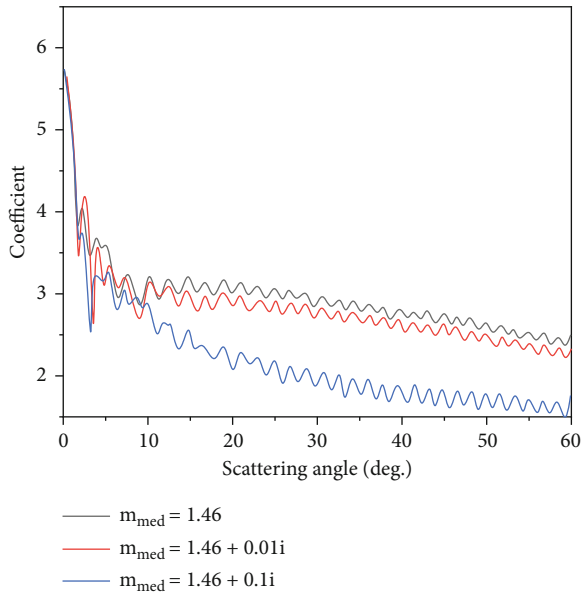

Figure 2: Mie scattering light intensity distribution under different medium absorption coefficients.

is 532 nm. Figure 4 is the scattering intensity diagram under the condition of 532 nm wavelength and 10 μm bubble radius.

It can be seen in Figure 4 that the scattering intensity of particles has a considerable peak at 0°, which indicates that the forward scattering of light by particles is very strong, but a strong backscattering can also be seen at 180°, which indicates that the backscattering of laser by bubbles can be used to detect microbubbles in water [13]. Under ideal conditions, when photons move in water, particles are evenly distributed. After controlling the laser wavelength, emission angle, and energy, the laser beam is emitted. The laser beam enters the water, and the motion state of photons can be understood by calculating the motion path and motion state of photons. Here, it is assumed that there is a free motion process between two adjacent collisions between a photon and a medium particle, and the photon only collides with the medium or particle [14]. According to Lambert's law and the principle of probability and statistics of the propagation of a collimated beam in a medium, the random sampling method for calculating the free path l_p of photon motion can be obtained as follows:

$$l_p = -\frac{\ln \xi}{c}, \tag{11}$$

where ξ is a random number evenly distributed among (0,1). The energy change of the collimated beam passing through the transmission medium is shown in Figure 5.

Then, the scattering angle of a single photon can be calculated by using the method of probability and statistics. By analogy, if we master the information of each free movement process of photons, we can obtain the clear trajectory of their movement in the medium.

3.3. Motion Law of Particles in Water. The motion of solid particles in water is mainly manifested in two categories: natural sedimentation and Brownian motion.

3.3.1. Natural Sedimentation. For spherical solid particles with density ρ_s and particle size D, they move in an infinite volume liquid with density ρ_f and viscosity η. Because the density of solid particles is significantly greater than that of liquid, the particles will naturally settle in the liquid, making the instantaneous settling velocity of particles u [15]. At this time, the particles are subjected to three forces: gravity w in the vertical downward direction, buoyancy F_a in the vertical upward direction, and flow resistance F_D in the vertical upward direction opposite to the settling speed, as shown in Figure 6.

Of course, the above movements are based on the following assumptions:

(a) Particles are spherical rigid bodies. Obviously, during the movement of gaseous particles, due to different pressures, the particle size will change. Obviously, gaseous particles will rise faster and faster in the process

(b) The motion is the motion of isolated particles, and the motion of particles is not affected by other particles

(c) In the process of particle sedimentation, the liquid moves in a simple laminar flow and the Reynolds number of the complex flow involves high-level knowledge of fluid mechanics, which cannot be simply expressed

(d) The container of the liquid is infinite, and the sedimentation of particles will not be affected by the edge effect of the liquid near the wall. At the same time, the liquid maintains a constant temperature to ensure that the density does not change [16]

3.3.2. Brownian Motion. When the particles move in the liquid, they will be impacted not only by gravity, buoyancy, and flow resistance but also by the continuous and irregular impact caused by the thermal movement of surrounding liquid molecules. According to the theory of molecular kinematics, the thermal motion of molecules is never ending. At any temperature, liquid molecules (including gas molecules) themselves will constantly make irregular random thermal motion, called Brownian motion, and hit the surface of the object at a high speed and high frequency. For example, for air molecules, the impact per square centimeter at room temperature is about 2.9×10^{23} times/second, and for particles with particle size ηm suspended in the air, the impact per second is about 1016 times. Similarly, when particles are dispersed in liquid, they will also be impacted by liquid molecules [17]. In most cases, due to the mass difference between the impacted molecules and the impacted particles, the displacement of particles caused by them can be ignored. However, when the particle itself is small in size and small in mass, the impact caused by the thermal motion of surrounding molecules cannot be ignored. At this time, if the particle

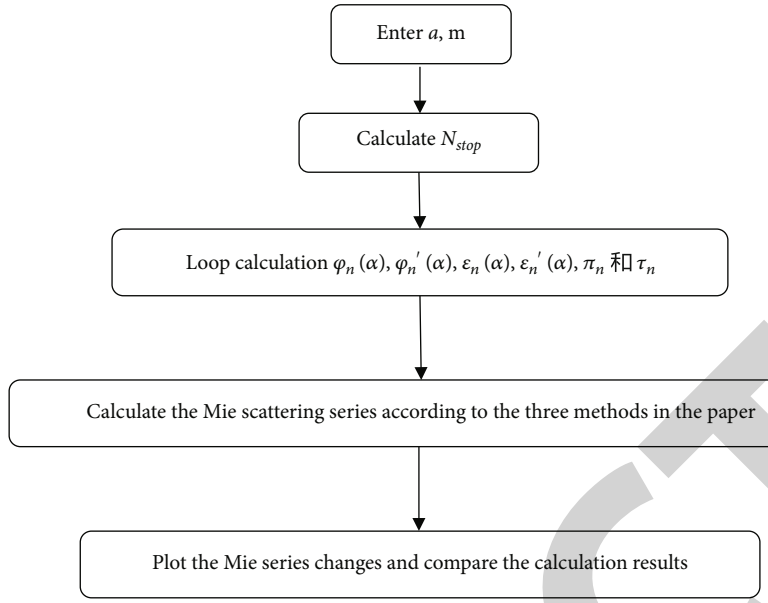

Figure 3: Procedure flow chart.

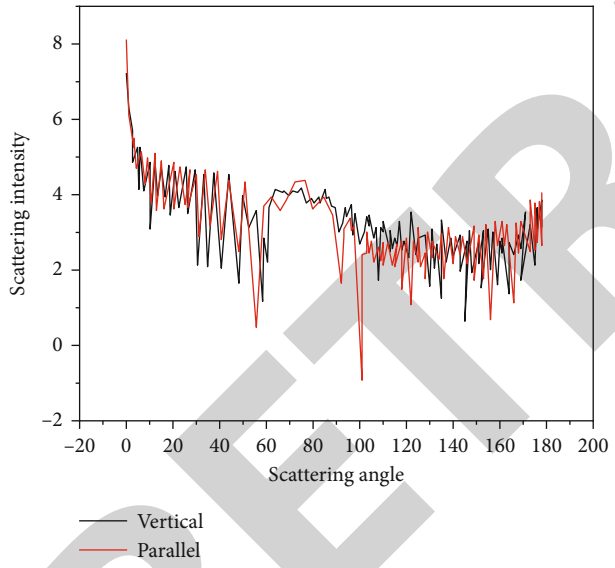

Figure 4: Light scattering intensity distribution of single bubble.

Figure 5: Collimated beam passing through transmission medium.

displacement is used to calculate the particle size, Brownian motion should be considered additionally.

3.4. Movement Law of Gaseous Particles (Bubbles) in Water. The force acting on the bubble in the medium solution is basically gravity and the buoyancy and viscous resistance of water to it. In the medium solution, the distance between any two bubbles can be considered to be large enough, and the bubbles will not interact with each other, nor will they rupture or merge.

4. Result Analysis

4.1. Dynamic Light Scattering Analysis Method. Bubbles are constantly moving in water, so when the laser beam is incident on the bubble group, the scattered light intensity changes with time due to the movement of bubbles. The more bubbles passing through the laser beam in a unit time, the faster the scattered light intensity changes. This provides a theoretical reference for measuring the velocity of bubbles through the change frequency of scattered light intensity. In the experiment, we collected the scattered light signal in a period of time through CMOS image sensor and then obtained the average moving speed of the bubble group through the signal analysis method [18].

Next, the dynamic light scattering analysis is carried out. Because the images are collected continuously in the experiment, each image is successively in time. In this way, the average gray level of each image is calculated (it marks the relative size of the scattered light intensity), and then, the change law with time is drawn. Figure 7 shows the change of laser-scattered light with time when there are no bubbles in the water. It can be seen that the scattered light intensity is still changing, but the difference between the maximum light intensity and the minimum light intensity is no more than 0.3, mainly because there are small impurities in the water, which also produce scattered light. Because they are relatively stable, the scattered light changes slightly, and they are the main factors of noise.

When there are bubbles in the pool, the pressure of the inflation pump is 0.03 MPa. At this time, the detection distance is 0.5 m, and the incident height of the laser beam is 0.4 m. There are a lot of moving bubbles in the water. At this

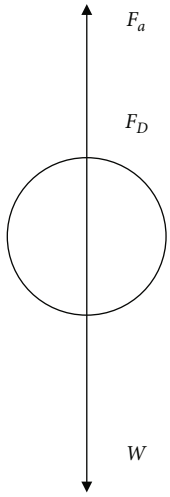

Figure 6: Stress diagram of spherical particle sedimentation movement.

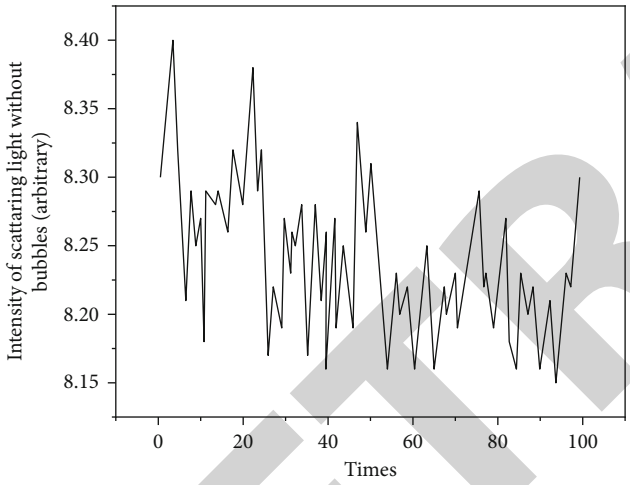

Figure 7: Variation of scattered light intensity with time when there is no bubble.

time, the laser beam is incident into the water, and then, the scattered light image is collected by the CMOS image sensor. In these four consecutive frames of images, it can be seen that there is a scattering halo outside the focus with alternating light and dark. This is consistent with the previous scattering pattern analyzed according to the light scattering theory. The different rings in the figure represent the scattered light intensity of different scattering angles [19]. We also use the dynamic light scattering method to draw the variation diagram of scattered light intensity with time according to the continuously collected images. Figure 8 shows the change of laser scattering light intensity of the bubble group with time. It can be seen that when there are a large number of moving bubbles in the water, the backscattered light intensity increases significantly, and the light intensity is also changing rapidly. The existence of bubbles greatly increases the scattered light intensity. The maximum

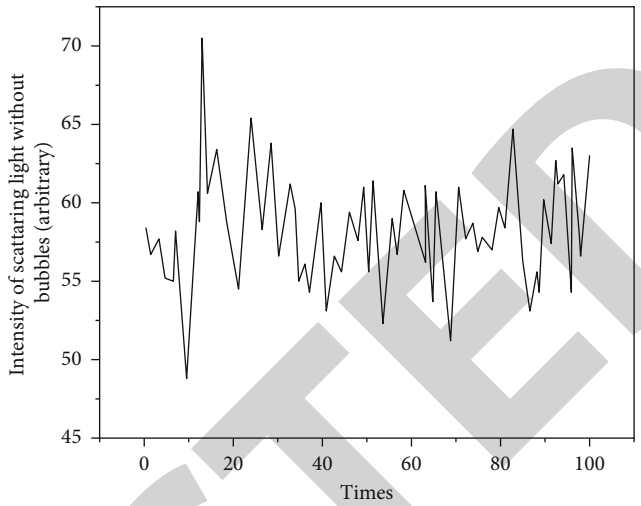

Figure 8: Variation of scattered light intensity with time in the presence of bubbles.

scattered light intensity (relative value) in Figure 7 does not exceed 9, while the minimum scattered light intensity (relative value) in Figure 8 is more than 40, so the light scattering characteristics of bubbles are very obvious. The experiment shows that it is feasible to detect the wake by laser.

It can be seen in Figures 7 and 8 that the dynamic light scattering signal changes randomly in the time domain. It is difficult to analyze the change law of the signal in the time domain; that is, it is difficult to get the information of the physical parameters of the bubble group [20]. At this time, we use the method of signal analysis in the frequency domain to convert the signal in time domain into the signal in the frequency domain, so that we can clearly see which frequency signal accounts for the main part [21]. The method of fast Fourier transform is used in data processing. At present, the fast Fourier transform method proposed by Willert is widely used. The MATLAB mathematical calculation tool is selected as the data processing software. Figure 9 shows the energy density diagram when there are no bubbles in the water. It can be seen from the figure that when there are no bubbles in the water, the energy of the signal is very low, and it can be clearly seen that the low-frequency part of the signal accounts for most of the energy. That is to say, the noise caused by impurities in water is mainly concentrated in the low-frequency part, and the frequency of this part is less than 15 Hz [22]. This is very helpful for our future experiments. During data acquisition, we can design a high pass filter to filter out low-frequency impurity signals, so as to obtain more accurate bubble group scattered light signals.

Figure 10 shows the variation of energy density of the scattered light signal of the bubble group with frequency. It can be seen from the figure that the existence of bubbles makes the scattered light energy rise sharply, which is consistent with the change of scattered light intensity explained by the signal change in the time domain. From the figure, it can be seen that there are mainly four kinds of frequency signals in the signal, which are 15 Hz, 26 Hz, 36 Hz, and 47 Hz

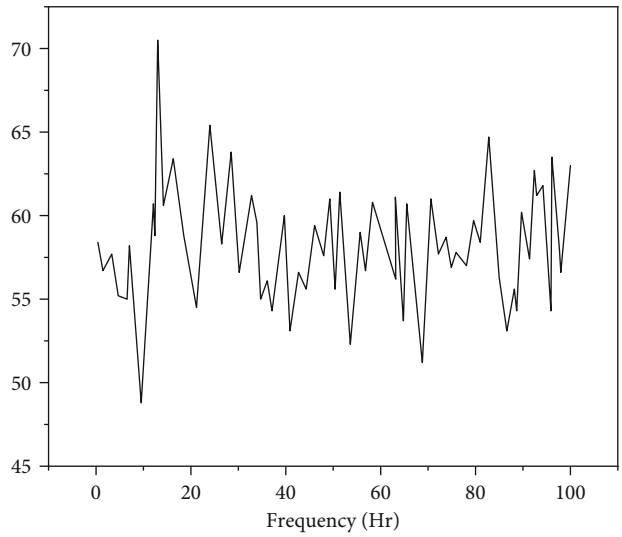

Figure 9: Error diagram of scattered light energy when there is no bubble.

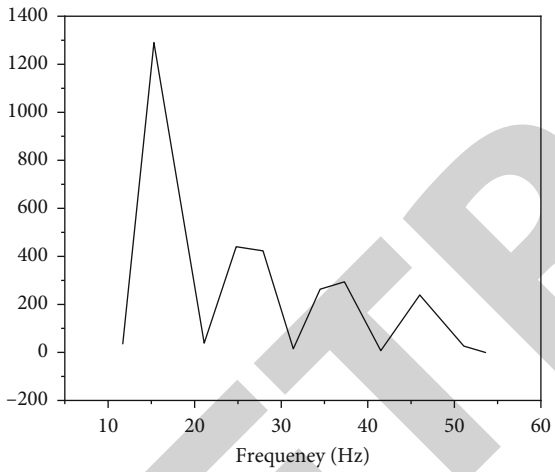

Figure 10: Error diagram of scattered light energy when there are bubbles.

in numerical order. When there is no bubble, the scattered light signal is mainly caused by small impurities in the water. From the previous analysis, it is known that this part of the signal is mainly concentrated in the low-frequency part (the frequency is below 15 Hz). When there is a bubble, the signal with medium frequency greater than 15 Hz occupies most of the energy of the signal. This part of the signal is the dynamic scattered light signal caused by the bubble that we want to analyze.

Figure 11 shows the variation law of the bubble rising speed and its diameter in this experiment. It can be seen from the figure that when the bubble diameter is less than 1000, the bubble rising speed has a basic linear relationship with the diameter. The data in the references and the conclusion obtained by analyzing the experimental data are basically credible. The average velocity of the bubble group can be obtained by the dynamic light scattering method and

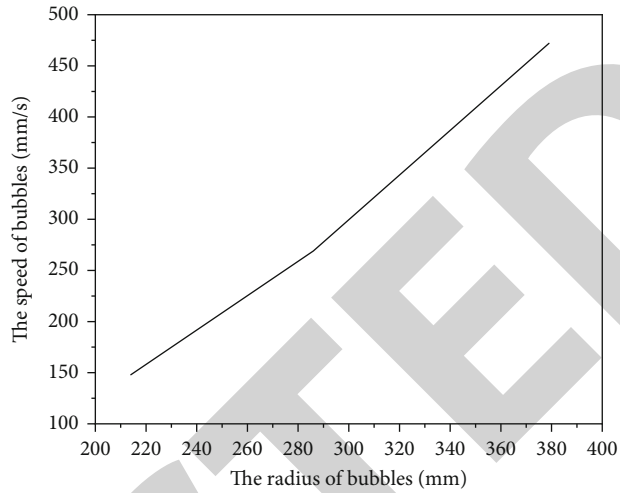

Figure 11: Relationship between bubble velocity and diameter.

Fourier frequency spectrum analysis method, and then, the diameter of the bubble can be obtained according to Stokes' law of the bubble in still water [23].

In the laboratory, the height of the laser can be adjusted to change the incident height of the laser beam, so that the moving speed and diameter of the bubble group at different depths can be calculated. I will not list them one by one here due to space limitations. Using the dynamic light scattering method to analyze the physical parameter information of the bubble group has many advantages from the above analysis and calculation. First of all, the experimental conditions are not very demanding. The key of the experiment is to adjust the rear focal plane of coos and Fourier lens. As long as they can be adjusted to the same position, the signal can be collected. Secondly, this experiment is an indirect measurement experiment, which has great advantages over the direct method of taking bubble motion images and then using image processing. Its calculation amount is very small, and the main calculation focuses on the fast Fourier transform. For the high-speed performance of modern computers, the time required to adopt the fast Fourier transform is very short, and the intuitive image analysis method is greatly affected by the performance of CCD. The calculation results largely depend on the quality of the captured image, and the depth of focus of the optical system is easy to cause image blur, so when there are a large number of bubbles, it is not advisable to use the intuitive image analysis method. Finally, this method uses the signal processing method in the frequency domain, which can quickly extract the main movement speed in the bubble group. In terms of signal acquisition, the real size of the scattered light intensity is not required; only the change law of the scattered light intensity with time is required, so the detection distance of the laser can reach 2 m in the experiment. The calculated results are obtained under laboratory conditions, which have certain reference significance for the bubble characteristics in the real wake. Of course, because the laboratory is carried out under very ideal conditions, such as water and sea water in the pool are still very different, whether the simulated

bubbles are similar to those in the wake remains to be verified. Using dynamic light scattering analysis method cannot get the density distribution of bubbles, only the velocity and diameter of bubbles.

4.2. Static Light Scattering Analysis Method. Because the previous dynamic light scattering analysis method cannot get the density of bubbles, this paper attempts to use the static light scattering analysis method. In the experiment, CMOS is used to collect the scattered light intensity spectrum of the bubble group. In the previous analysis, the dynamic analysis method is used to analyze the transformation law of the scattered light of the bubble group in a short period of time to obtain the moving speed of the bubble group. Here, the nature of a signal at a certain time is specially analyzed during data processing; that is, we only analyze the image of a certain frame. This is the static light scattering analysis method. The image sensor used in the experiment is a CMOS image sensor of type A602f/fc produced by the German Basel company. The maximum resolution of the sensor is 656×491, the pixel size is $9.9\,\mu\text{m} \times 9.9\,\mu\text{m}$, the output format is 8 bits/pixel, and the maximum frame rate at the highest resolution is 100 fps. You can reduce the resolution to improve the frame rate. The resolution of the images collected in this experiment is 640×480, and the images collected are 8-bit gray-scale images.

4.2.1. Principle of Ring Division. Since the focus is at the center of the left edge of the image, according to the previous optical path analysis, it is known that each ring should take the center of the left edge, that is, the focus as the center of the circle. Because the bright spot near the focus is too strong, the scattered light intensity has been completely submerged, so the starting position of the ring is the cut-off position of the bright spot, and the ring thickness is determined by the size of a single CMOS pixel and the previous $dr \approx -f\,du$ formula. The MATLAB mathematical calculation tool is used to calculate the sum of all pixel values contained in each ring, which represents the measured angular scattered light intensity. At the same time, the theoretical value of the measured angle can be calculated according to Mie's light scattering theory. Comparing the results of the two methods, we can get whether the experiment is correct or not. The halo division in image processing adopts the principle of linear division. From $dr \approx -f\,du$ to $\Delta r \approx -f\square\Delta u$, the focal length f of the Fourier lens in the experiment is 30 mm. When the scattering angle increases by 0.2 degrees, $\Delta r = 0.2 \times 30 \times \pi/180 \approx 0.1$ mm, and the size of a single CMOS pixel is $9.9\,\mu\text{m} \times 9.9\,\mu\text{m}$; that is, the thickness B of the halo is about 10 pixels. Divide the image according to this thickness and the starting position of the halo analyzed above, and then, calculate the sum of all pixel values contained in each ring and compare it with the calculation results of the Mie scattering theory. The comparison results are shown in Figure 12. In principle, the more the number of rings is divided in image processing, the more sampling points will be obtained, and the data can more accurately represent the variation law of scattering intensity with the scattering angle. From this point of view, double the number

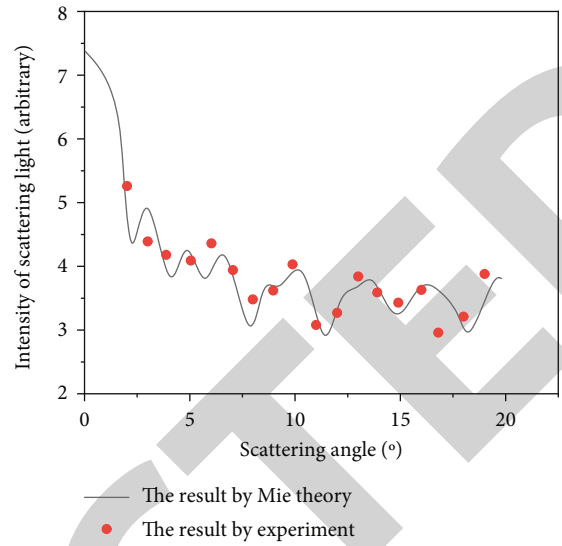

Figure 12: Comparison between the processing result of 10-pixel-thick halo and the result of Mie theory.

of halos; that is, take 5 pixels as the thickness of a halo. According to the previous calculation, the scattering angle increases by about 0.1 degrees. Of course, the starting position of the halo is the same as the previous one.

Figure 12 shows the comparison between the experimental results of the division method with the halo thickness of 10 pixels and the theoretical results of meter scattering. From the figure, it can be seen that the experimental results are basically consistent with the theoretical results, but there is a large deviation in individual points. The main reason is that the thickness of the halo is too large, and the sum of the pixel values is not only the scattered light intensity of a single angle, but the integral of the scattered light intensity to a certain angle range. In order to reduce the error, only the thickness of the halo can be reduced. Reduce the thickness of the halo by one time; that is, the thickness of the halo is 5 pixels. Divide the halo according to this thickness, and then, calculate and compare it with the result of the Michel theory, as shown in Figure 13. It can be seen from the figure that the experimental results are very consistent with the theoretical results. The reduction of the thickness of the halo makes the included angle range very small, so the integral effect of the scattered light intensity on the angle can be ignored. It can be seen that the ring thickness in image processing has an impact on the results. In order to get better experimental results, the ring thickness should be within 10 pixels, but from another point of view, the reduction of the ring thickness will inevitably lead to the increase of the number of rings, which will increase the difficulty of image processing and calculation. When selecting, we should comprehensively consider the accuracy and time complexity. Figures 12 and 13 well illustrate that it is feasible to use the CMOS image sensor to receive and detect scattered light in this experiment. The forward scattered light of bubbles shows a downward trend as the scattering angle increases. The scattered light intensity is the largest near zero, and the scattered light intensity has a nonlinear relationship with the

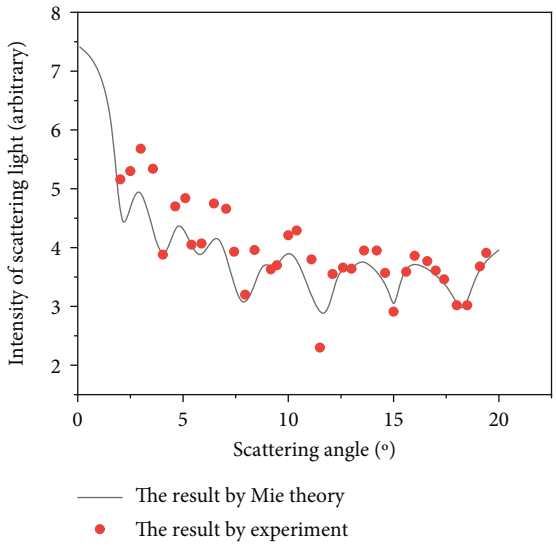

Figure 13: Comparison between the processing result of 5-pixel-thick halo and the result of Mie theory.

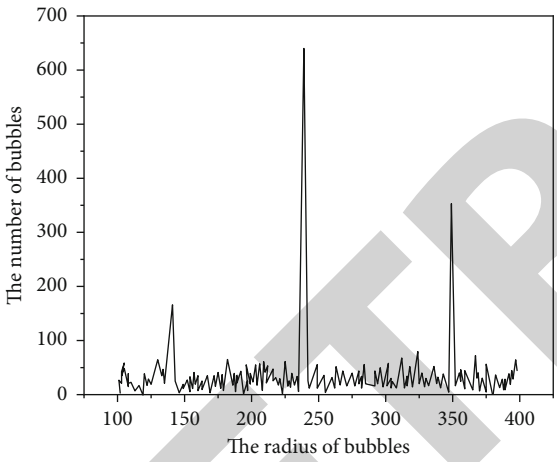

Figure 14: Distribution of bubble number under projection inversion algorithm ($h = 0.4$ m).

scattering angle. From the above analysis, it is known that the experimental results are roughly consistent with the theoretical results, so the diameter of bubbles can be deduced from the correct experimental results. The inversion algorithm is used here. The projection iterative algorithm is used in data processing in this paper [24]. The bubble diameter information obtained from the inversion of the scattered light intensity of the bubble group is shown in Figure 14. It can be seen in Figure 14 that the diameter of the main bubbles in the bubble group is about 240 μm, accounting for about 50% of the whole bubble group in number, the bubbles with a diameter of about 140 μm account for 24% of the whole bubble group, and the bubbles with a diameter of about 350 μm account for 24% of the whole bubble group. These data are based on the incident height of the laser beam at 0.4 m, which is half the depth of the pool. Appropriately increase the incident height of the laser beam ($h = 0.6$ m)

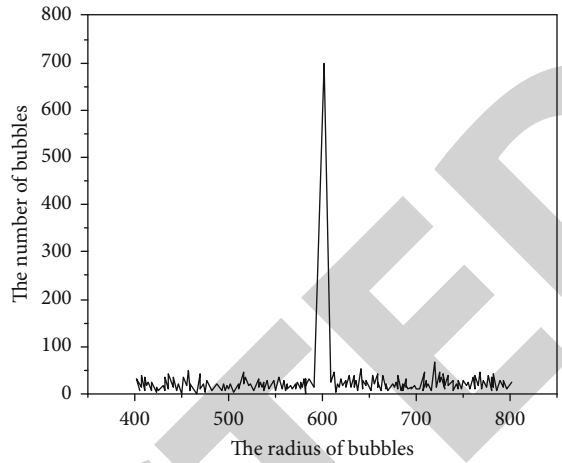

Figure 15: Distribution of bubble number under projection inversion algorithm ($h = 0.6$ m).

to detect bubbles in shallow waters. After data processing, the number distribution of bubble groups is shown in Figure 15 [25]. It can be seen from the figure that in shallow water, the diameter of bubbles is larger and the number of bubbles in deep water is reduced. This is because bubbles rupture and merge during the rising process, some bubbles dissolve in the water, and the air pressure in shallow water increases, and bubbles expand and deform, so the diameter of bubbles is larger, about 600 μm.

5. Conclusion

Through the analysis of dynamic and static light scattering signals, the physical parameter information of the bubble group can be obtained, such as bubble velocity, bubble diameter, and bubble group distribution density. The method of fast Fourier transform is used in dynamic light scattering signal processing, and good results are obtained. The static light scattering signal is filtered and preprocessed before processing, and the diameter and density of bubbles are obtained through the inversion algorithm. Through the above theoretical calculations and experimental results, we believe that it is completely feasible to use optical methods to study wake bubbles and track the target according to this, but we still need to further study the light scattering characteristics of bubble groups.

Data Availability

The datasets used during the current study are available from the corresponding author on reasonable request.

Conflicts of Interest

The author declares that the research was conducted in the absence of any commercial or financial relationships that could be construed as a potential conflict of interest.

Acknowledgments

This work was sponsored in part by the following fund project: in 2020, the school level scientific research project of Shanghai Jianqiao University was approved (project name: application of Mie theory in new light scattering materials; project number: sjq20001).

References

[1] H. Xu, W. Zhang, J. Deng, and J. Rabault, "Active flow control with rotating cylinders by an artificial neural network trained by deep reinforcement learning," *Journal of Hydrodynamics*, vol. 32, no. 2, pp. 254–258, 2020.

[2] N. B. Khan, Z. B. Ibrahim, M. A. Ali et al., "Numerical simulation of flow with large eddy simulation at re = 3900," *International Journal of Numerical Methods for Heat & Fluid Flow*, vol. 30, no. 5, pp. 2397–2409, 2020.

[3] W. Pan, X. Chen, G. Dai, and F. Wang, "Enhanced effect of bubble deformation on internal particle transport," *Industrial and Engineering Chemistry Research*, vol. 59, no. 2, pp. 905–918, 2020.

[4] Q. Xiao, B. Yza, B. Xla, and B. Jza, "Unsteady experimental and numerical investigation of aerodynamic performance in ultra-high-lift LPT," *Chinese Journal of Aeronautics*, vol. 33, no. 5, pp. 1421–1432, 2020.

[5] L. Yan, K. Cengiz, and A. Sharma, "An improved image processing algorithm for automatic defect inspection in TFT-LCD TCON," *Nonlinear Engineering*, vol. 10, no. 1, pp. 293–303, 2021.

[6] Q. Li, J. Xu, Y. Kamada et al., "Experimental investigations of airfoil surface flow of a horizontal axis wind turbine with ldv measurements," *Energy*, vol. 191, p. 116558, 2020.

[7] M. R. Mcgrory, M. D. King, and A. D. Ward, "Using Mie scattering to determine the wavelength-dependent refractive index of polystyrene beads with changing temperature," *The Journal of Physical Chemistry A*, vol. 124, no. 46, pp. 9617–9625, 2020.

[8] G. Li, F. Liu, A. Sharma et al., "Research on the natural language recognition method based on cluster analysis using neural network," *Mathematical Problems in Engineering*, vol. 2021, Article ID 9982305, 13 pages, 2021.

[9] V. Bhullar, S. Sardana, and A. Mahajan, "Size modeling of TiO_2 nanofibers for efficient TiO_2 sensitized mesoscopic solar cells," *Solar Energy*, vol. 230, pp. 177–185, 2021.

[10] C. Sandin and L. Mattsson, "Three-component modelling of C-rich AGB star winds – V. effects of frequency-dependent radiative transfer including drift," *Monthly Notices of the Royal Astronomical Society*, vol. 499, no. 2, pp. 1531–1560, 2020.

[11] I. L. Rasskazov, P. S. Carney, and A. Moroz, "Intriguing branching of the maximum position of the absorption cross section in Mie theory explained," *Optics Letters*, vol. 45, no. 14, pp. 4056–4059, 2020.

[12] W. J. Kim, A. Mesbah, X. Deschanels, S. Bernard, and S. Lebègue, "First principles investigations of the optical selectivity of titanium carbide-based materials for concentrating solar power applications," *Journal of Materials Chemistry C*, vol. 9, no. 24, pp. 7591–7598, 2021.

[13] A. Jc, B. Jl, L. B. Xin, A. Wg, Z. Jing, and C. Fza, "Degradation of toluene in surface dielectric barrier discharge (SDBD) reactor with mesh electrode: Synergistic effect of UV and TiO_2 deposited on electrode," *Chemosphere*, vol. 288, article 132664, 2022.

[14] M. Mungra, Y. Li, M. Pravettoni, and A. Lennon, "Impact of angular irradiation profiles on performance of silicon pv modules using light scattering films," *IEEE Journal of Photovoltaics*, vol. 11, no. 3, pp. 750–759, 2021.

[15] M. N. Mustafa and Y. Sulaiman, "Review on the effect of compact layers and light scattering layers on the enhancement of dye-sensitized solar cells," *Solar Energy*, vol. 215, no. 11, pp. 26–43, 2021.

[16] Q. Q. Zhu, S. Li, Q. Yuan, H. Zhang, and L. Wang, "Transparent YAG:Ce ceramic with designed low light scattering for high-power blue LED and LD applications," *Journal of the European Ceramic Society*, vol. 41, no. 1, pp. 735–740, 2021.

[17] Z. Sci, "Piecewise sparse recovery via piecewise inverse scale space algorithm with deletion rule," *Journal of Computational Mathematics*, vol. 38, no. 2, pp. 375–394, 2019.

[18] F. Gürsoy, M. Ertürk, and M. Abbas, "A picard-type iterative algorithm for general variational inequalities and nonexpansive mappings," *Numerical Algorithms*, vol. 83, no. 3, pp. 867–883, 2020.

[19] Z. Tian, T. Wang, M. Giles, E. K. Butker, and S. T. Kahn, "Evaluation of a multiresolution-level inverse planning algorithm for non-invasive radiosurgery for vestibular schwannoma," *International Journal of Radiation Oncology • Biology • Physics*, vol. 108, no. 3, pp. e273–e274, 2020.

[20] R. Huang, "Framework for a smart adult education environment," *World Transactions on Engineering and Technology Education*, vol. 13, no. 4, pp. 637–641, 2015.

[21] L. H. Nguyen, "A new algorithm to determine the creation or depletion term of parabolic equations from boundary measurements," *Computers & Mathematics with Applications*, vol. 80, no. 10, pp. 2135–2149, 2020.

[22] L. Reichel and U. O. Ugwu, "Tensor krylov subspace methods with an invertible linear transform product applied to image processing," *Applied Numerical Mathematics*, vol. 166, pp. 186–207, 2021.

[23] X. Zhang, Y. Zhou, H. Zheng et al., "Reconfigurable metasurface for image processing," *Nano Letters*, vol. 21, no. 20, pp. 8715–8722, 2021.

[24] B. Chen, H. Li, W. Luo, and J. Huang, "Image processing operations identification via convolutional neural network," *SCIENCE CHINA Information Sciences*, vol. 63, no. 3, pp. 1–3, 2020.

[25] M. Bradha, N. Balakrishnan, A. Suvitha et al., "Experimental, Computational Analysis of Butein and Lanceoletin for Natural Dye-Sensitized Solar Cells and Stabilizing Efficiency by IoT," *Environment, Development and Sustainability*, vol. 24, no. 6, pp. 8807–8822, 2022.